Child's Nervous System (2019) 35:315–328
https://doi.org/10.1007/s00381-018-3984-6

ORIGINAL ARTICLE

Expression profiles of pro-inflammatory and pro-apoptotic mediators in secondary tethered cord syndrome after myelomeningocele repair surgery

Gesa Cohrs[1] · Bea Drucks[1] · Jan-Philip Sürie[1] · Christian Vokuhl[2] · Michael Synowitz[1] · Janka Held-Feindt[1] · Friederike Knerlich-Lukoschus[1,3]

Received: 26 June 2018 / Accepted: 21 September 2018 / Published online: 3 October 2018

Abstract

Purpose The literature on histopathological and molecular changes that might underlie secondary tethered cord syndrome (TCS) after myelomeningocele (MMC) repair surgeries remains sparse. To address this problem, we analyzed specimens, which were obtained during untethering surgeries of patients who had a history of MMC repair surgery after birth.

Methods Specimens of 12 patients were analyzed in this study. Clinical characteristics were obtained retrospectively including pre-operative neurological and bowel/bladder-function, contractures and spasticity of lower extremities, leg and back pain, syringomyelia, and conus position on spinal MRI. Cellular marker expression profiles were established. Further, immunoreactivities (IR) of IL-1ß/IL-1R1, TNF-α/TNF-R1, and HIF-1α/-2α were analyzed qualitatively and semi-quantitatively by densitometry. Co-labeling with cellular markers was determined by multi-fluorescence-labeling. Cytokines were further analyzed on mRNA level. Immunostaining for cleaved PARP and TUNEL was performed to detect apoptotic cells.

Results Astrocytosis, appearance of monocytes, activated microglia, and apoptotic cells in TCS specimens were one substantial finding of these studies. Besides neurons, these cells co-stained with IL-1ß and TNF-α and their receptors, which were found on significantly elevated IR-level and partially mRNA-level in TCS specimens. Staining for HIF-1α/-2α confirmed induction of hypoxia-related factors in TCS specimens that were co-labeled with IL-1ß. Further, hints for apoptotic cell death became evident by TUNEL and PARP-positive cells in TCS neuroepithelia.

Conclusions Our studies identified pro-inflammatory and pro-apoptotic mediators that, besides mechanical damaging and along with hypoxia, might promote TCS development. Besides optimizing surgical techniques, these factors should also be taken into account when searching for further options to improve TCS treatment.

Keywords Dysraphism · Cytokines · Real-time RT-PCR · Hypoxia

Gesa Cohrs and Bea Drucks contributed equally to this work.

Portions of this work were presented in abstract form and in oral presentation at the 44th Congress of the International Society for Pediatric Neurosurgery, Kobe, Japan, October 24, 2016 and in abstract form and in poster form at the 68th Congress of the German Society for Neurosurgery, Magdeburg, Germany, May 16, 2017.

✉ Friederike Knerlich-Lukoschus
f.knerlich@asklepios.com

[1] Department of Neurosurgery, University Hospital of Schleswig-Holstein Campus Kiel, Arnold-Heller-Str. 3, House 41, 24105 Kiel, Germany

[2] Department of Pathology, University Hospital of Schleswig-Holstein Campus Kiel, Arnold-Heller-Str. 3, House 14, 24105 Kiel, Germany

[3] Deparment of Pediatric Neurosurgery, Asklepios klinik Sankt Augstin GmbH, Arnold-Janssen-Str. 29, 53757 Sankt Augustin, Germany

Abbreviations

CD3	Cluster of differentiation 3
CD11b/Integrin αM	Cluster of differentiation 11b
CD68	Cluster of differentiation 68
CKPan	Cytokeratin Pan
CNPase	2′,3′-Cyclic nucleotide 3′-phosphodiesterase
cPARP	Cleaved poly-ADP-ribose polymerase
CSF	Cerebrospinal fluid
CT	Cycle of threshold
DAB	Diaminobenzidine
GAPDH	Glyceraldehyde-3-phosphate dehydrogenase
GFAP	Glial fibrillary acidic protein
H&E	Hematoxylin-eosin
HIF	Hypoxia-inducible factor
IHC	Immunohistochemistry
IL-1ß	Interleukin-1 beta
IL-1R1	Interleukin-1 beta receptor type 1
IR	Immunoreactivity
MMC	Myelomeningocele
NeuN	Neuronal nuclear protein
NF200kD	Neurofilament 200-kD fragment
RT	Room temperature
RT-PCR	Reverse transcription polymerase chain reaction
SD	Standard deviation
SDS	Sodium dodecyl sulfate
TCS	Tethered cord syndrome
TNF-α	Tumor necrosis factor alpha
TNF-R1	Tumor necrosis factor receptor type 1
TUNEL	Terminal deoxynucleotidyl transferase-mediated dUTP-biotin nick end labeling

Introduction

About 10 to 30% of patients who underwent myelomeningocele (MMC) repair surgery after birth develop TCS-related symptoms in their further clinical course [1–4]. Symptoms typically include development or worsening of lower-limb motor deficits, sensory deficits, bladder dysfunction, and musculoskeletal deformities [5–7].

The underlying mechanical causes are varied and, in regard to post MMC repair, include scar formation with consecutive adhesion and tension of neural structures at the site of surgical reconstruction [8–10]. Therefore, continuing efforts addressed in particular surgical aspects such as dura repair to prevent adhesion of neural structures to the surrounding arachnoid space [11, 12]. However, despite development of sophisticated surgical methods, there is no technique that can reliably prevent SC tethering after MMC repair [5]. Secondary TCS after MMC repair cannot be reduced to mechanical problems alone, as some patients do not benefit from an untethering surgery. Besides improving surgical techniques, it is therefore important to investigate further cellular and molecular mechanisms that potentially underlie clinical relevant TCS.

Hypoxia has been identified as one such factor for clinically relevant TCS. Thereby, distraction of the SC is thought to lead to vascular compromise with ischemic alterations occurring especially in the gray matter [8, 9, 13–15]. The degree of oxidative metabolism impairment has been shown to be predictive for neurological improvement after untethering surgeries [10, 16]. Yamada et al. demonstrated that TCS is associated with metabolic abnormalities at the level of cytochrome α,α3, which reflects impaired mitochondrial function in compromised neuronal cells [17]. Further hints for neural damage were provided recently by Maurya et al.'s clinical investigations in which biomarkers of neuronal damage (S100B) and glia activation (GFAP) were elevated in the CSF of patients operated for primary TCS [18].

Considering our recent studies on cellular and molecular alterations in MMC placodes [19], inflammation might be a further crucial factor in secondary TCS. Compared to normal SC, MMC placodes exhibited significantly elevated GFAP- and Vimentin-immunoreactivity. In addition, chemokines and cytokines, crucial mediators of secondary lesion cascades after SC injury, were found on elevated mRNA and immunoreactivity level. These processes might also be relevant for the development of TCS after MMC repair surgeries.

To check this hypothesis, we now analyzed histological material, which was obtained during secondary untethering surgeries of patients who initially underwent MMC repair in their first days of life. Specimens that were obtained during untethering of placodes from surrounded scar tissue were investigated for inflammatory cellular and molecular alterations along with expression of hypoxia-inducible factors (HIF) 1α and 2α. Because inflammation and hypoxia are involved in apoptotic mechanisms, expression of cPARP (cleaved poly-ADP-ribose polymerase) was investigated as apoptotic-related mediator [20], besides terminal deoxynucleotidyl transferase-mediated dUTP-biotin nick end labeling (TUNEL).

Material and methods

Ethical review was obtained from the Clinical Research Ethics Board of the University of Schleswig-Holstein, Kiel, Germany (AZ.: AD 430/15).

Tissue specimens and clinical characteristics

The electronic neuropathological and clinical databank was queried for cases operated for TCS. From these cases, only patients who had a history of MMC repair after birth were considered.

Because tissue samples were obtained during untethering of placodes from the surrounded scarred tissue, hematoxylin- and eosin-stained (H&E) sections of identified cases were screened for probes that harbored neuroepithelial fragments. These cases were then processed further as described in the following sections.

The respective clinical charts were reviewed retrospectively. Control specimens for immunohistochemistry and real-time RT-PCR included lumbar SC tissue from adults for whom no spinal pathology was documented ($n = 4$).

Histology and immunohistochemistry

Details on the staining protocols were reported previously [19]. Antibody specification and dilutions are provided in Table 1. Sections were mounted with Rotimount® (Roth, Karlsruhe, Germany) and coverslipped for investigation under a Zeiss light microscope (Axiovert; Carl Zeiss AG, Jena, Germany). Sections of different patients were stained simultaneously, and DAB reactions were precisely timed to ensure comparability.

Table 1 Cellular marker and cytokine/cytokine receptor antibodies used for immunohistochemistry

Marker	Specificity	Epitope/immunogen/dilution	Source
Cytokines and cytokine-receptors			
cPARP	Cleaved poly-ADP-ribose polymerase	116 kDa Nuclear poly (ADP-ribose) polymerase, 1:200	Cell Signaling Technology, Danvers, MA, USA; Cat.#9541
HIF-1α	Hypoxia-inducible factor 1-alpha	Fusion protein made to an internal sequence of human HIF1-alpha, 1:100	Novus Biologicals, Littleton, CO, USA; Cat.#NB100-134
HIF-2α	Hypoxia-inducible factor 2-alpha	Peptide derived from the C-terminus of mouse/human HIF-2 α protein, 1:100	Novus Biologicals, Littleton, CO, USA; Cat.#NB100-122
IL-1b	Interleukin-1ß	Amino acids 117-269 of IL-1ß of human origin, 1:100	Santa Cruz Biotechnology, Santa Cruz, CA, USA; Cat.#sc-7884
IL-1RI	Interleukin 1 receptor, type 1	Peptide mapping at the C-terminus of IL-1RI, 1:500	Santa Cruz Biotechnology, Santa Cruz, CA, USA; Cat.#sc-689
TNF-alpha (L-19)	Tumor necrosis factor alpha	Peptide mapping at the N-terminus of TNF-alpha of mouse origin; polyclonal goat IgG, 1:100	Santa Cruz Biotechnology, Santa Cruz, CA, USA; Cat.#sc-1351
TNF-R1	Tumor necrosis factor receptor	Epitope mapping between amino acids 427-454 at the C-terminus of TNF-R1 of mouse origin	Santa Cruz Biotechnology, Santa Cruz, CA, USA; Cat.#sc-374185
Phenotypic marker antibodies			
CD3	T cells, inflammatory cells	13-mer Peptide corresponding to 156-168 of the epsilon chain of human CD3 protein, 1:100	Thermo Fisher Scientific, Fremont, CA, USA; Cat.#RM-9107
CD11b (OX-42)	Microglia, macrophages	Rat peritoneal macrophages, mouse monoclonal IgG, 1:50	Morphosys AbD GmbH (Serotec), Düsseldorf, Germany; Cat.#MCA275G
CD68 (ED1)	Macrophages, monocytes	Single chain glycoprotein of 90-100 kDa; mouse monoclonal IgG, 1:100	Morphosys AbD GmbH (Serotec), Düsseldorf, Germany; Cat.#MCA341R
CNPase	2′,3′-Cyclic nucleotide 3′-phosphodiesterase; oligodendrocytes	Full length native protein, mouse monoclonal IgG, 1:1000	Biozol, Eching, Germany; Cat.#ab6319
GFAP	Glial fibrillary acidic protein	Mouse GFAP, mouse monoclonal mouse IgG, 1:100-1:500	Millipore/Chemicon, Schwalbach, Germany, Cat.#3402
NeuN	Neuron-specific nuclear protein (neuronal nuclei)	Cell nuclei from mouse brain, mouse monoclonal IgG, 1:1000	Millipore/Chemicon, Schwalbach, Germany, Cat.#377
NF-200	Neurofilament (200 kDa); neuronal cells	Carboxy-terminal tail of porcine H-chain, mouse monoclonal IgG, 1:1000	Millipore/Chemicon, Schwalbach, Germany, Cat.#5266
Synaptophysin	Neuroendocrine marker synaptophysin	Synthetic peptide of synaptophysin, 1:50	Thermo Fisher Scientific, Fremont, CA, USA; Cat.#RM-9111
Vimentin	Intermediate filament Vimentin	Epitope localized on the coil-2 part of the Vimentin rod domain, 1:200	DAKO, Glostrup, Denmark; Cat.#M7020

Table 2 Clinical and imaging characteristics of TCS patients

Case #	Sex	Age at surgery	MMC	Motor function	Back pain	Leg pain	BB dysfunction	Syrinx	Max. diameter of syrinx, mm	Syrinx expansion (vertebral segments)	Conus position
1	m	19 mo	Lumbosacral	Progressive lower-limb deformity	–	–	Worsening	Yes	6	4	L3/4
2	m	5 mo	Lumbosacral	Progressive lower-limb deformtiy	–	–	Worsening	Yes	4	4	L4/5
3	f	46 y	Lumbosacral	Known pareses	–	Yes	Yes	–	–	–	L5
4	f	7 y	Lumbosacral	Leg pain	–	Yes	Yes	–	–	–	L1
5	m	8 y	Lumbar	Known pareses	–	–	Yes	–	–	–	L4
6	f	3 y	Lumbar	pp (known), progressive spasticity	–	–	Yes	–	–	–	L4/5
7	f	12 y	Thoracolumbar	pp (known)	–	–	Yes	–	–	–	L2
8	f	11 y	Lumbar	pp (known	–	–	Yes	–	–	–	L2
9	f	3 y	Thoracolumbar	progressive pp	–	–	Yes	Yes	5	3	L5
10	f	2 y	Lumbar	pp	–	–	Yes	–	–	–	L4
11	f	16 mo	Thoracolumbar	pp (known)	–	–	Yes	Yes	3	7	L3
12	f	21 y	Lumbar	Sensory deficit lower limbs, known pareses	Yes	–	Normal	–	–	–	L4/5

BB bowel/bladder, *f* female, *m* male, *mo* months, *y* years, *pp* paraplegic

Controls included 1) omission of the first antibody; 2) staining with mouse, rabbit, and goat isotype IgG (monoclonal mouse IgG; MAB002 [R&D Systems, Minneapolis, MN]; monoclonal rabbit IgG; ab37415 [Abcam, Cambridge, MA];

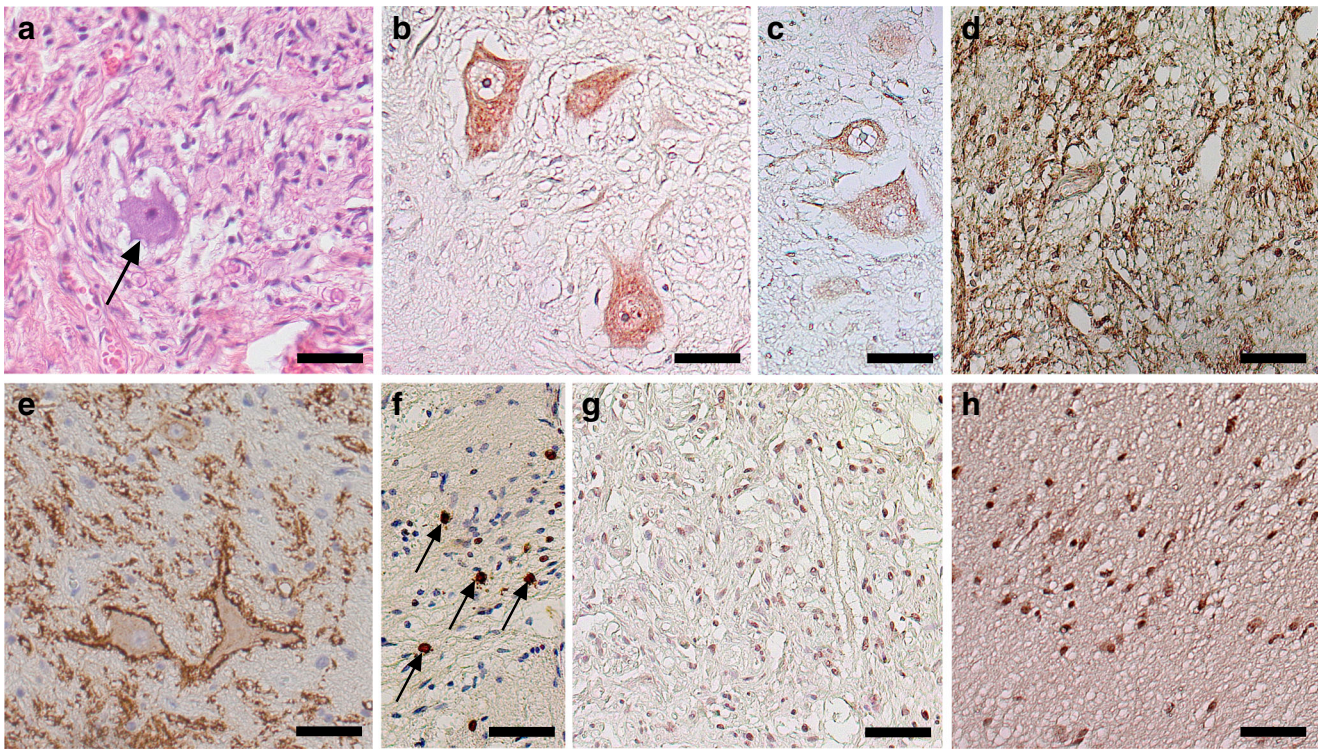

Fig. 1 Immunohistochemical expression patterns of phenotypic markers in TCS neuroepithelia. **a** H&E-stained TCS specimen depicting, among others, cells with neuronal morphology in neuroepithelial tissue element (arrow). Immunostaining confirmed neuronal cells by NeuN (**b**) and NF200kD (**c**) labeling. Cells positive for the oligodendroglial marker CNPase were found in neuroepithelial parts of TCS specimens (**d**). Synaptophysin showed a granular staining pattern around neuronal structures in the neuroepithelium (**e**). CD3 (**f**), CD11b (**g**), and CD68 (**h**) positive inflammatory cells (arrows in (**f**)) and microglial cells in neuroepithelial structures of TCS cases. Scale bars 100 μm in all images

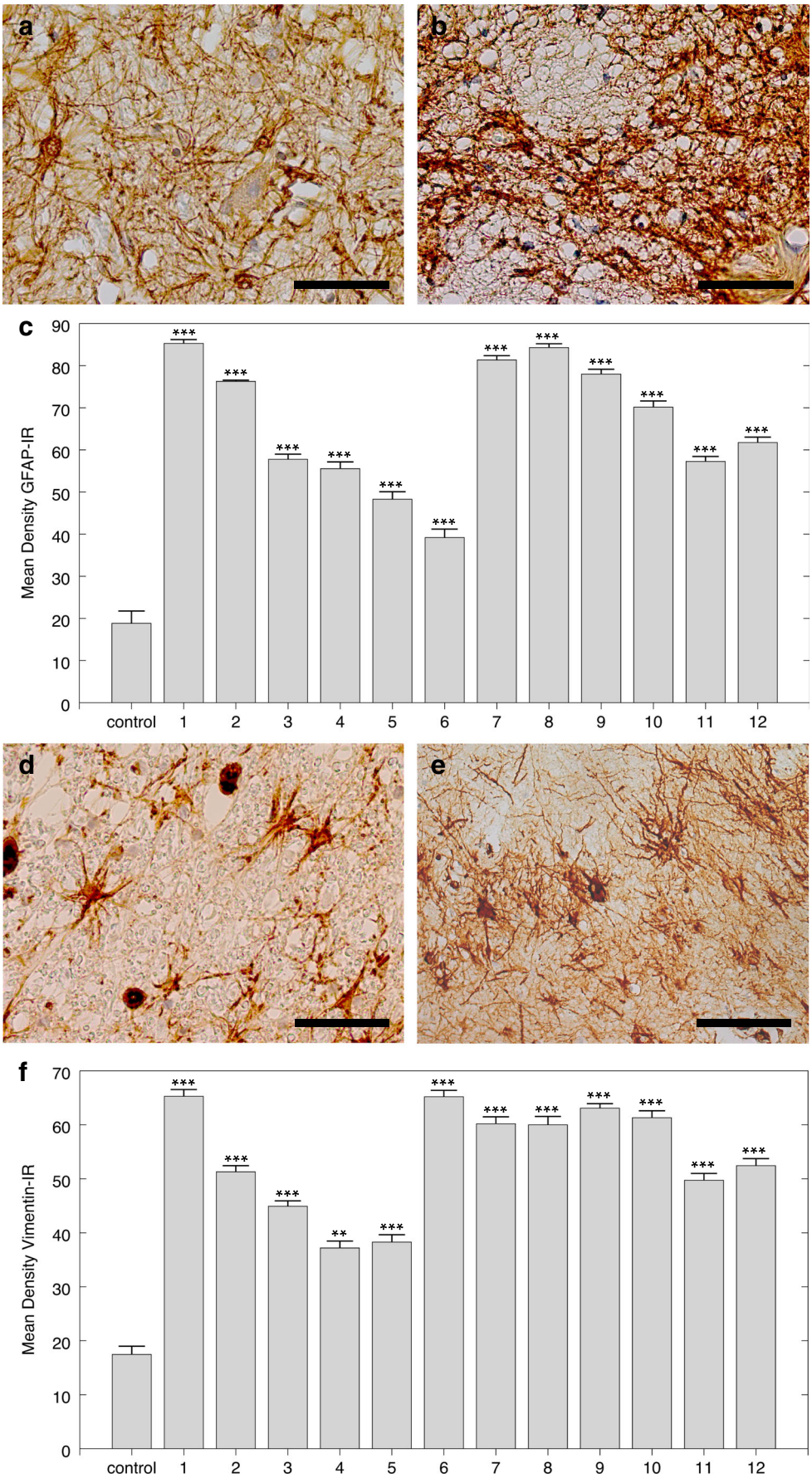

Fig. 2 GFAP and Vimentin immunoreactivity in TCS neuroepithelia. GFAP-immunoreactivity in adult SC control sections (**a**) compared to neuroepithelial regions of TCS specimens (**b**). GFAP-IR density was significantly higher in TCS cases compared to adult SC controls (**c**): Integrated GFAP-IR densities were plotted for each case and pooled for adult SC control tissue. Vimentin IR was found in adult SC-specimens (**d**) and TCS-specimens (**e**). **f** Densitometric measurements verified elevated Vimentin IR in TCS cases compared to control specimens. Significant differences are indicated by * in comparison to control specimens (significance level $**p < 0.01$, $***p < 0.001$). Scale bar 50 μm in all images

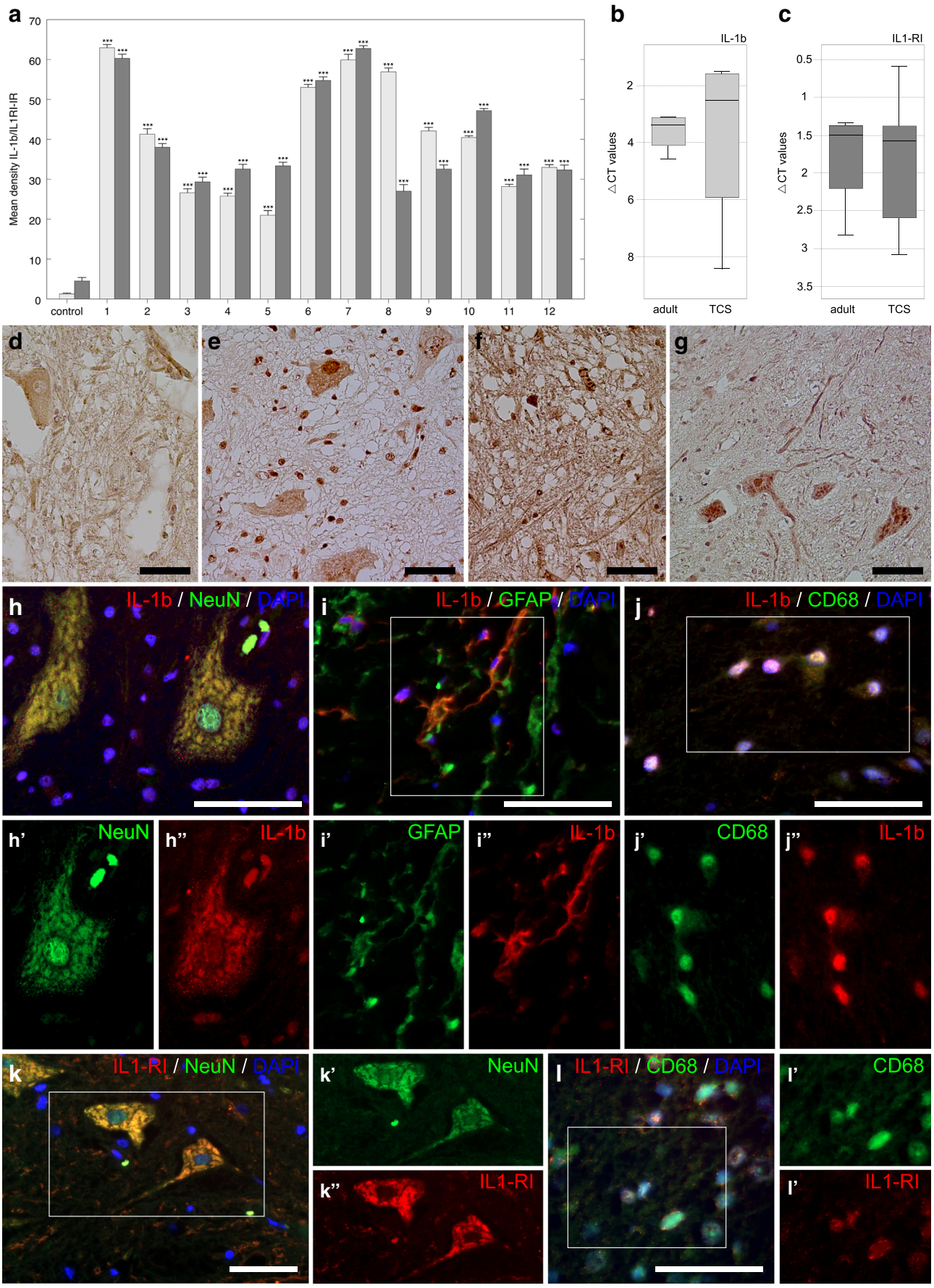
a
Mean density IL-1b/IL1RI-IR
control
1
2
3
4
5
6
7
8
9
10
11
12
b
IL-1b
△CT values
adult
TCS
c
IL1-RI
△CT values
adult
TCS
d
e
f
g
h
IL-1b / NeuN / DAPI
i
IL-1b / GFAP / DAPI
j
IL-1b / CD68 / DAPI
h'
NeuN
h''
IL-1b
i'
GFAP
i''
IL-1b
j'
CD68
j''
IL-1b
k
IL1-RI / NeuN / DAPI
k'
NeuN
k''
IL1-RI
l
IL1-RI / CD68 / DAPI
l'
CD68
l'
IL1-RI

◀ **Fig. 3** Expression of IL-1ß and its receptor in TCS neuroepithelia. Immunoreactivity density levels for IL-1ß and its ligand are shown in (A) compared to adult controls. IL-1ß- and IL-1RI-IR densities were significantly higher compared to adult SC controls (significance level $***p < 0.001$). On mRNA level, IL-1ß (B) and IL-1RI (C) exhibited a tendency towards higher mRNA-expression levels in TCS cases compared to adult SC controls. However, this did not reach statistical significant levels (delta CT values are demonstrated as boxplots for mRNA expression in adult SC- and TCS-tissues). Morphologically control sections exhibited faint IL-1ß-IR (D), whereas TCS sections revealed strong IR for IL-1ß-IR (E). There was no IL-1RI detectible on control sections (F). Neuroepithelia in TCS specimens showed immunoreactive cellular structures, which exhibited glial and neuronal morphology (G). Co-staining reconfirmed these findings, demonstrated in (H) with co-expression of IL-1ß (red) and NeuN (green) (upper panel merged image with IL-1ß (red)/NeuN (green)/nuclear staining (DAPI, blue), lower left panel green channel for NeuN (green) staining, lower right panel red channel for IL-1ß-IR). (I) Co-staining for IL-1ß (red) and GFAP (green) (merged upper panel, lower panels separated channels) confirmed astroglial expression pattern. Co-staining of IL-1ß (red) and CD68 (green) in clusters of inflammatory cells are shown in (J) (merged channels in the upper panel, lower panels separated channels). (K) Double-immunofluorescence staining confirmed co-staining of IL-1R1-IR and neuronal marker NeuN (merged channel in left image; single channel images depicting staining for NeuN as green signal (upper panel) and for IL-1R1 as red signal (lower panel)). Further IL-1R1-IR was co-stained with microglial/macrophage-marker CD68 in (L) (merged channel in left image; single channels for CD68 (green) in the upper panel and for IL-1R1 (red) in the lower panel). Scale bars in all images 50 μm

monoclonal goat IgG; AB-108-C [R&D Systems, Minneapolis, MN]); and 3) performing IL-1ß and IL-1RI IHC on anonymized encephalitis brain specimens.

TUNEL staining was applied to visualize DNA fragmentation in apoptotic cells (#11684817910, Roche Applied Science). Sections were deparaffinized, rehydrated, boiled in citrate buffer, and immersed in TritonX-100/hydrogen peroxidase. Non-specific staining was reduced by incubating sections with 3% bovine serum albumin/Tris buffered saline (1 h; room temperature) before applying TUNEL (terminal deoxynucleotidyl transferase-mediated dUTP-biotin nick end labeling) reaction mixture (1 h, 37 °C in humid chambers). After washing, converter-peroxidase was incubated on the slides for 30 min at 37 °C. Labeling was visualized with DAB substrate (Sigma, Taufkirchen, Germany). Negative controls were performed by omitting the TUNEL reaction mixture. Apoptosis was assessed by light microscopy. Cell death rates were calculated by counting positive cells on fixed areas (5 × 5 mm).

Densitometry for semi-quantitative measurement of immunoreactivities

GFAP-, Vimentin-, IL-1ß-, IL-1RI-, TNF-α-, TNF-R-, and HIF-1α/2α-IR were analyzed semi-quantitatively as described previously [19].

Immunofluorescence-multi-labeling procedures

Cytokines and their receptors were stained in combination with anti-NeuN (1:500), anti-GFAP (1:500), and anti-CD68/ED1 (1:200). IL-1ß and HIF-1/2α were multi-labeled with NeuN. Details on the staining procedures were reported previously [21]. After incubation with the first primary antibodies against NeuN and IL-1ß, sections were stained with anti-rabbit Alexa Fluor 555 (donkey, polyclonal, 1:1000; Invitrogen) and anti-mouse Alexa Fluor 488 (donkey, polyclonal, 1:1000; Invitrogen) as second primary antibodies. After incubation with the second primary antibody (IL-1ß), the second secondary antibody was anti-rabbit Alexa Fluor 647 (donkey, polyclonal, 1:1000; Invitrogen). After embedding in Immu-Mount (Shandon, Pittsburgh, PA), fluorescence was observed under an Axiovert 200 Zeiss microscope and Axiovert Observer with Zeiss ApoTome.2 attachment (Carl Zeiss, Oberkochen, Germany). Pictures were taken both of fluorescence-imaged sections and overlaid using AxioVision software (Carl Zeiss GmbH, Jena, Germany).

mRNA preparation and real-time RT-PCR

IL-1ß-, IL-1R1-, TNF-α-, and TNF-R-mRNA amounts in TCS specimens ($n = 6$) and in control ($n = 4$) SC tissues were measured by real-time RT-PCR as described previously [22]. TaqMan primer probes (assays on demand; Applied Biosystems, Foster City, CA) were used. RNAs of individual samples were isolated with High Pure FFPET RNA Isolation Kit (Roche Diagnostics GmbH, Mannheim, Germany) from ten paraffin sections of 5 μm thickness per case. Areas of interest and lumbar SC of controls were scratched from the slides. Eight hundred microliters Xylene (RotiClear, Roth, Karlsruhe, Germany) and 400 μL ethanol were added to the dissected tissue.

Real-time PCR was performed on each sample using a Quantstudio® 5 Single Color Real-time PCR detection system (Applied Biosystems by ThermoFisher Scientific, USA) and TaqMan primer probes (assays on demand; GAPDH, Hs99999905_m1; IL-1ß, Hs01555410_m1; IL-1RI, Hs00991010_m1; TNF-α, Hs00174128_m1; TNF-R Hs01042313_m1; Applied Biosystems, Foster City, CA) using a total reactive volume of 20 μL, which contained 1 μL of 20×Target Assay Mix, 10 μL of 2×TaqMan Universal Master Mix, and 100 ng of cDNA template (diluted in RNase free water to 9 μL). After 10 min at 95 °C for polymerase activation, 50 cycles of 15 s at 95 °C (denaturation) and 1 min at 60 °C (annealing and extension) were run. Glyceraldehyde-3-phosphate dehydrogenase (GAPDH) was used as intrinsic positive control and normalizer. The cycle of threshold (C_T) of each sample was averaged, and ΔCT values were calculated as C_T [Gene of interest] − C_T [GAPDH].

Statistical analyses

Results are expressed by means ± SD. Statistical test was performed at the α level of significance of 0.05 by two-tailed analysis using parametric tests. Test of factors including pair-wise comparisons was applied with the Student's *t* test. Data management and statistical analysis were performed using SPSS (version 22.0; IBM, Inc., Somers, NY) and Microsoft® Excel 2007.

Results

Clinical characteristics

By analyzing H&E-stained specimens, 12 cases were identified that harbored sufficient neuroepithelial tissue for further analysis. Clinical characteristics of these patients are summarized in Table 2. All patients underwent a second surgery for clinically relevant secondary TCS after being initially operated for open spinal dysraphism after birth. On presurgical MRI imaging, most cases presented with low-lying conus except case 4 (lumbar level L1) and cases 7 and 8 (lumbar level L2). Four patients exhibited progressive syrinx formation of varied extent.

Immunohistochemical marker expression profile of specimens under investigation

By analyzing H&E sections, tissue specimens, which contained neuroepithelial elements, were identified for further investigations. Only specimens that contained cells with neuronal morphology (Fig. 1a) exhibiting NeuN-staining (Fig. 1b) and neuronal NF-staining (Fig. 1c) were included in this study. CNPase as a marker for oligodendroglial cells was also confirmed in TCS specimens (Fig. 1d). Synaptophysin as an integral membrane glycoprotein present in presynaptic vesicles in neurons was traced in all cases (Fig. 1e). Round inflammatory cells, positive for CD3 and CD11b, were present in nine out of 12 cases (Fig. 1f, g). CD68 was detected in all 12 cases (Fig. 1h).

Strong GFAP-immunoreactivity (IR) was found in all TC specimens compared to control sections (Fig. 2a, b). Densitometry confirmed a significant GFAP induction in TC specimens (Fig. 2c). This was paralleled by Vimentin IR, which was strongly expressed in TC specimens compared to control SC sections (Fig. 2d, e) with significant higher IR densities ($p < 0.001$) in all 12 cases (Fig. 2f). In regard to morphological features of GFAP- and VIM-positive astrocytes, cells in TC specimens appeared with thickened cellular processes and pronounced cell bodies, as a hint for an activated cell state.

Expression of IL-1/IL-1R1b and TNF-α/TNF-R

IL-1ß-/IL-1RI-IR was detectable in all TCS cases with a highly significant induction when compared to SC control sections ($p < 0.001$) (Fig. 3A). On mRNA level, IL-1ß was also found on elevated level compared to control SC samples (Fig. 3B), IL-1RI showed no significant difference in mRNA expression (Fig. 3C). Morphological appearances of IL-1ß- and IL-1R1-IR in control and TC specimens are shown exemplarily in Fig. 3: There were no specific IL-1ß staining patterns in adult SC (Fig. 3D), but strong IL-1ß-IR in cells scattered throughout the neuroepithelia (Fig. 3E). These cells exhibited morphological neuronal and microglial characteristics. In adult, SC IL-1RI remained immuno-negative (Fig. 3F) compared to strong IL-1R1 IR in TC specimens (Fig. 3G). Double-immunofluorescence labeling confirmed co-staining of IL-1ß with NeuN (Fig. 3H), and co-staining in subsets of cells labeled with GFAP (Fig. 3I) and CD68 (Fig. 3J). Double-fluorescence labeling also confirmed co-staining of IL-1RI and NeuN (Fig. 3K), as well as IL-1RI and CD68 (Fig. 3L).

Staining of TNF-α in adult SC sections showed no specific staining (Fig. 4A); in TCS cases, neuronal staining patterns were detected (Fig. 4B). TNF-R-IR remained negative in staining of adult SC controls (Fig. 4C). TNF-R-IR was confined to cells resembling neurons (Fig. 4D). TNF-α and its receptor TNF-R were found on significantly higher immunoreactivity density level in TC specimens compared to adult SC controls (Fig. 4E). Corresponding to IHC results, the investigation on mRNA level showed a tendency towards higher mRNA expression of TNF-α in TCS cases compared to adult SC controls (Fig. 4F). TNF-R expression on mRNA level was significantly elevated in TCS specimens compared to controls (Fig. 4G). TNF-R and NeuN were co-stained in double-immunofluorescence labeling of TCS specimen (Fig. 4H).

Expression patterns of hypoxia-inducible factors

A highly significant elevation of HIF-1α-/-2α-IR in TCS specimens compared to SC controls was detected in all TCS cases (Fig. 5A). Staining of HIF-1α/-2α was not specific in SC controls (Fig. 5B, C); in contrast, structures of neuronal resemblance were detected in TCS specimens by staining of HIF-1α (Fig. 5D) and HIF-2α (Fig. 5E). Double-immunofluorescence labeling proved co-staining of NeuN and HIF-1α (Fig. 5F) and CD68 and HIF-1α (Fig. 5G). NeuN co-stained with HIF-2α in TCS specimens (Fig. 5H). Multi-immunofluorescence labeling revealed co-staining of NeuN, HIF-2α, and pro-inflammatory cytokine IL-1ß (Fig. 5I).

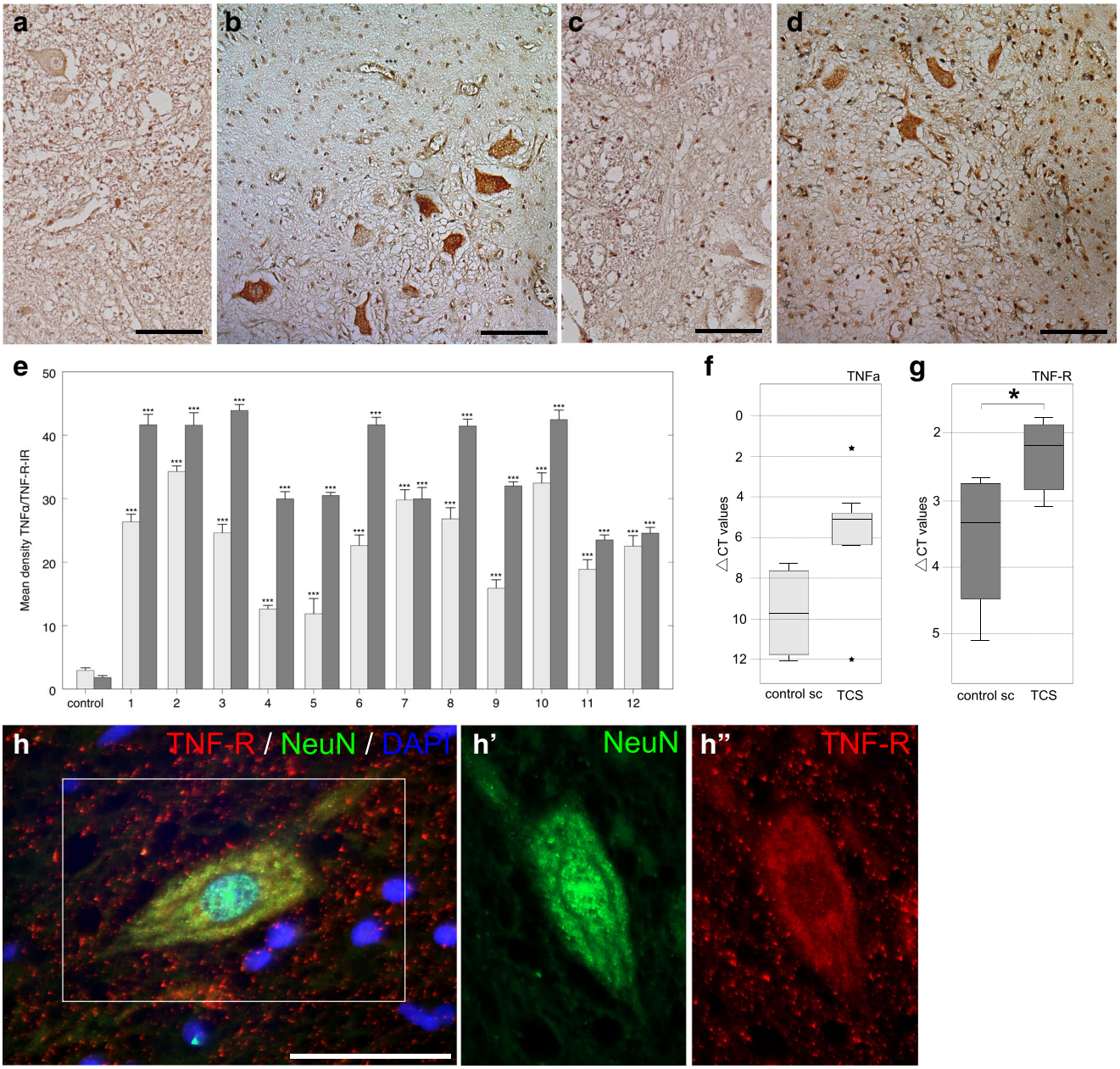

Fig. 4 Expression of TNF-α and TNF-R in TCS neuroepithelia. Faint TNF-α staining in adult control specimens (A) compared to intense TNF-α-IR in TCS neuroepithelia (B) and expression patterns of the respective TNF-R in SC control (C) and TCS specimens (D). In (E) TNF-α-/R-IR, integrated mean densities are plotted for adult controls and TCS neuroepithelia (significance level $***p < 0.001$). (F) On mRNA level, TNF-α was not significantly induced in TCS compared to adult SC specimens, which contrasted the significantly higher induction of TNF-R1 on mRNA level compared to adult SC specimens (G) (significance level $*p < 0.05$). Besides inflammatory cells, there was double labeling for TNF-R (red) and NeuN (green) (DAPI, blue) (H). Scale bars A–D 100 μm, H 50 μm

Apoptotic markers in tethered cord syndrome specimens

Staining with cPARP was not specific in SC control sections (Fig. 6a). Structures positive for cPARP showed morphologic features of apoptotic cell fragments scattered through the investigated sections that were positive for neuroepithelial markers (Fig. 6b). Whereas staining with TUNEL on control sections showed no specific staining (Fig. 6c), there were TUNEL-positive fragments in TCS specimens (Fig. 6d). However, the number of TUNEL-positive cells in fixed areas did not statistically differ between TCS and control cases (Fig. 6e).

Discussion

By analyzing cellular marker expression profiles, it became evident that all TCS specimens exhibited significantly

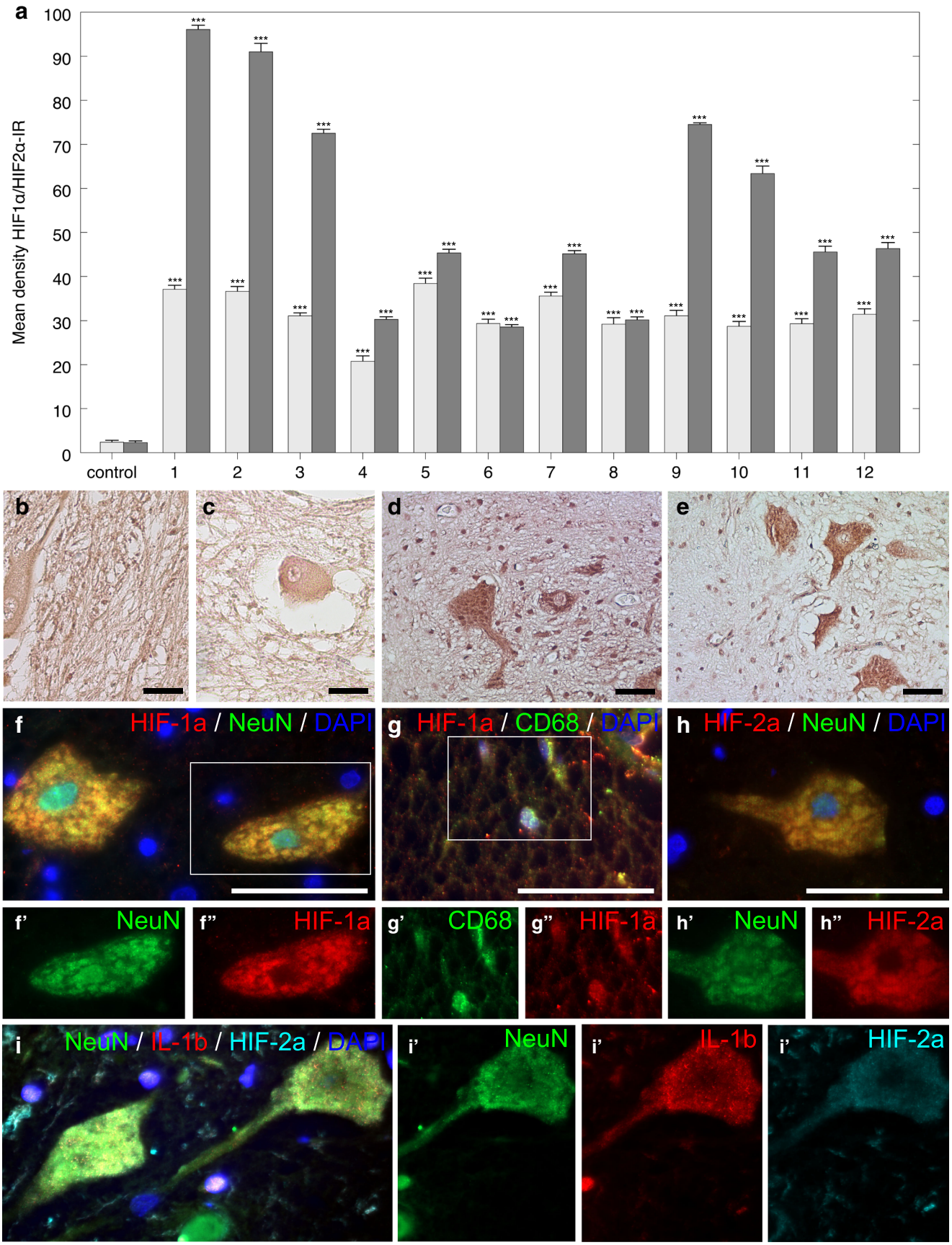
a
Mean density HIF1α/HIF2α-IR
100
90
80
70
60
50
40
30
20
10
0
control
1
2
3
4
5
6
7
8
9
10
11
12
***
b
c
d
e
f HIF-1a / NeuN / DAPI
g HIF-1a / CD68 / DAPI
h HIF-2a / NeuN / DAPI
f' NeuN
f'' HIF-1a
g' CD68
g'' HIF-1a
h' NeuN
h'' HIF-2a
i NeuN / IL-1b / HIF-2a / DAPI
i' NeuN
i' IL-1b
i' HIF-2a

◀ **Fig. 5** Expression of hypoxia-related molecules. (A) HIF-1α- and HIF-2-IR were detectable at significantly higher density levels in TCS specimens compared to adult control specimens (***$p < 0.001$ TCS compared to adult control sections). (B) HIF-1α-IR and (C) HIF-2α-IR in adult SC control specimens. (D) HIF-1α-IR and (E) HIF-2α-IR exhibited a morphologically neuronal staining pattern in TCS specimens. (F) Double-immunofluorescence labeling confirmed co-labeling of NeuN (green) and HIF-1α-IR (red) (merged image in the upper panel (plus DAPI, blue nuclear staining), lower left panel NeuN (green), lower right panel HIF-1α (red)). There was also co-staining of CD68 (green) and HIF-1α (red) (merged image in G in the upper panel (DAPI, blue nuclear staining), lower left panel CD68 (green), lower right panel HIF-1α (red)). HIF-2α exhibited similar co-staining with NeuN (H) (merged image in the upper panel (including DAPI, blue nuclear staining), lower left panel NeuN (green), lower right panel HIF-2α (red)). (I) Triple-immunolabeling confirmed co-staining for NeuN (green), IL-1ß (red), and HIF-2α (turquoise) (merged image on the left (DAPI = blue), followed by separated channels for NeuN (green), IL-1ß (red), and HIF-2α (turquoise). Scale bars in all images 50 μm

elevated GFAP- and Vimentin-immunoreactivities compared to control tissues with astrocytes exhibiting typical morphological features of activation. Similar findings have been observed in open spinal dysraphism [19, 23–27]. Besides activated astrocytes, the appearance of monocytes and activated microglia were one further finding of our studies. Compared to controls, most TCS specimens exhibited cellular staining for inflammatory markers like CD3, CD68, and CD11b. This might reflect an unspecific cellular response to stretch-induced injury by TCS or can be considered a component of secondary lesion cascades which typically occurs after SC injury [28, 29].

The detectable induction of IL-1ß and TNF-α plus their receptors in TCS specimens supports the hypothesis of secondary lesion cascades as these inflammatory cytokines typically orchestrate a complex array of responses after different SC lesions: These molecules are induced in response to varied insults to the central nervous system (for review [30]) and are involved among others in immune cell recruitment, promotion of astrogliosis and tissue scarring [28, 31], and induction of apoptotic processes [32, 33]. Consistent with our findings, similar injury-related processes may also contribute to delayed neurological deterioration in symptomatic TCS after MMC repair surgeries.

Another relevant finding of our studies was the co-expression of strongly elevated HIF-IR and pro-inflammatory and pro-apoptotic cytokines in TC specimens. It is assumed that neurological deterioration in TCS is in part caused by stretch-induced ischemia and deprivation of SC energy metabolism [8, 10, 14, 17, 33]. By using experimental in vivo distraction devices, Dolan et al. proved ischemia as an essential factor in the pathophysiology of TCS [14]. There was significantly reduced blood flow in the tethered SC segments and compromised spinal evoked potentials, which correlated with the applied forces on neural structures. By applying intraoperative blood-flow monitoring, Schneider et al. demonstrated reconstituted blood flow in the respective SC segments during untethering surgeries [16]. Specimens of our studies also exhibited strong immunoreactivity of HIF-1 and HIF-2α, which was co-stained with cytokines in subgroups of neuronal and glial cells. TNF-α and IL-1ß were shown to increase the accumulation and transcriptional activity of HIF-1α [34]. In their studies with transgenic mice that were lacking the IL-1R1, Basu et al. found reduced lesion extension after hypoxic insult in adult stroke models [35]. One regulatory site of the IL-1ß promoter includes, among others, HIF, that enables IL-1 mRNA to be transcribed very early in response to ischemic insults [36, 37]. IL-1ß is therefore classified as an early injury signal [30, 38], and hypoxia-inducible factors are considered sensible markers of clinical relevant hypoxic/ischemic episodes [39]. Thus, our findings with elevated HIF-1/-2α in TCS specimens are consistent with the findings of previous studies, which identified hypoxia as one relevant consequence of mechanical tension on the tethered SC [10, 16, 17].

Besides IL-1ß/IL-1R1, TNF-α and its receptor were found with high IR densities in TC specimens. TNF-α is a potent inflammatory mediator with pro-apoptotic characteristics [40, 41]. Like after SC injury, apoptotic processes might also play a role in lesions cascades, which are induced by traction or by the altered microenvironment of post-operative scar formation. In our study, TCS specimens exhibited clusters of TUNEL and PARP-positive cells.

With our approach, we cannot address the aspect of when these processes occur during the clinical course after MMC repair. Expression of cytokines and appearance of inflammatory cells might occur as acute alterations, which lead to neuronal cell loss with consecutive decline of neurological function. On the other hand—in regard to our previous work on MMC specimens obtained during the initial repair surgery—inflammation might also be considered a chronic aspect of (open) spinal dysraphism: Like after SC injury, induction of pro-inflammatory and pro-apoptotic mediators may influence the long-term outcome by promoting the development of varied complications of the affected individuals [42, 43]. This aspect underlines once more the importance of early mmc repair to prevent further molecular lesion cascades and thus chronic sequelae like secondary TCS. Thereby knowing the onset and time-courses of inflammatory or apoptotic lesion cascades is a prerequisite to define the optimal time-point of surgical interventions. Besides laboratory investigations in animal models [44], improving imaging techniques bear the potential to become an important tool to investigate the time-courses of cellular and molecular lesion cascades “in situ” in the spinal cord before and after mmc repair or TCS surgery in the respective patients [45, 46]. Knowing these probably time-dependent processes will facilitate the decision-making of when to operate in those conditions.

The notion that all these reactions are caused solely by surgical manipulation during untethering appears unlikely as induction of apoptotic cell death-related pathways is detectable earliest hours after tissue damage, and the preparation at the placodes

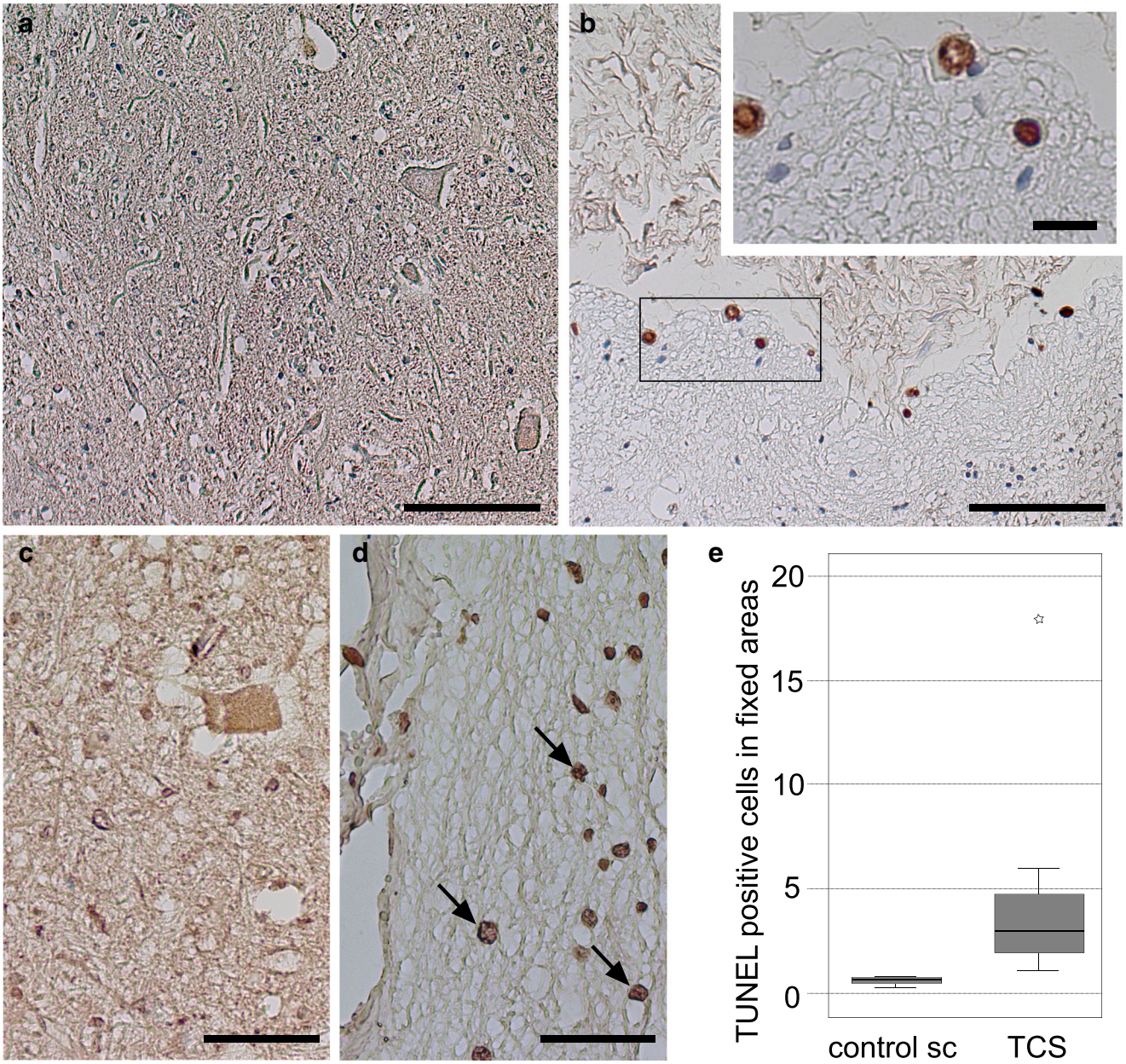

Fig. 6 Expression of apoptosis-related molecules and TUNEL of TCS neuroepithelia. No specific immunoreactivity (IR) for cleaved PARP (cPARP) was detectable in control spinal cord sections (**a**). In TCS specimens, cPARP-IR was found in small cellular fragments dispersed throughout the neuroepithelia (**b**) (higher magnification demonstrates cells which condensed or fragmented nuclei). To estimate the death rate, TUNEL-positive cells were counted in fixed areas in sections of control SC (**c**) and TCS specimens (**d**). There were differences which did not meet statistical significance, as shown in plot in (**e**) (number of positive cells (on *y*-axis) are plotted for SC controls ($n = 4$) and TCS specimens ($n = 12$ (*x*-axis)). Error bars represent standard error of the mean. Asterisk indicates outlier. Scale bars **a**–**b** 200 μm; inlay 20 μm, **c**–**d** = 50 μm

during untethering does usually afford less time. There are no studies available on post-surgical induction of inflammatory mediators in neurosurgical procedures. However, there are hints from other disciplines that selected cytokines (IL-β, IL-6, not TNF-a) may be elevated after surgery [47, 48]. Thus, in respect to the surgical technique, our findings may underline once more that a diligent clean and straightforward surgical strategy is essential in the operative management of dysraphic lesions: Blood products may promote, and prolonged surgeries may foster inflammatory reactions. Addressing this open question requires further investigations like determining cytokine serum levels before and after TCS surgery. Another approach would have been to investigate SC tissue obtained from "non-symptomatic" patients with morphological signs for TCS on MRI. For we do not promote "prophylactic" untethering in asymptomatic patients, such controls were unavailable.

Summary and conclusion

Our studies identified specific pro-inflammatory and pro-apoptotic mediators as further elements that, along with mechanical damaging and hypoxia, might underlie secondary TCS after MMC repair. Prevention of these lesion cascades by application of anti-inflammatory and anti-apoptotic factors in addition to a meticulous clean and straightforward surgical technique may result in a better outcome of secondary TCS. Due to its well-known anti-apoptotic, anti-inflammatory abilities and proven clinical applicability of its non-hematopoietic recombinant form, erythropoietin might be such a candidate [49–51]. The potential effect of such factors as adjuvant therapeutic agent in secondary TCS has to be examined in further studies.

Acknowledgments The authors thank Fereshteh Ebrahim, Brigitte Rehmke, and Silvia Iversen for their excellent technical assistance. At this point, we would also like to pay tribute to the memory of Professor Ivo Leuschner who, due to his expertise, cordiality and human warmth, had always been an esteemed discussion and cooperation partner, who passed away too soon in January 2017.

Funding information This work was funded by Familie Mehdorn Stiftung 2015 (to G.C. and F.K.L.).

Compliance with ethical standards

Conflict of interest No conflicts of interest concerning materials or methods used in this study or the findings specified in this paper exists.

References

1. Hertzler DA II, DePowell JJ, Stevenson CB, Mangano FT (2010) Tethered cord syndrome: a review of the literature from embryology to adult presentation. Neurosurg Focus 29:E1. https://doi.org/10.3171/2010.3.FOCUS1079
2. Bowman RM, Mohan A, Ito J, Seibly JM, McLone DG (2009) Tethered cord release: a long-term study in 114 patients. J Neurosurg Pediatr 3:181–187. https://doi.org/10.3171/2008.12.PEDS0874
3. Bowman RM, McLone DG, Grant JA et al (2001) Spina bifida outcome: a 25-year prospective. Pediatr Neurosurg 34:114–120. https://doi.org/10.1159/000056005
4. Shurtleff DB, Duguay S, Duguay G, Moskowitz D, Weinberger E, Roberts T, Loeser J (1997) Epidemiology of tethered cord with meningomyelocele. Eur J Pediatr Surg 7(Suppl 1):7–11. https://doi.org/10.1055/s-2008-1071200
5. Hudgins RJ, Gilreath CL (2004) Tethered spinal cord following repair of myelomeningocele. Neurosurg Focus 16:E7
6. Lew SM, Kothbauer KF (2007) Tethered cord syndrome: an updated review. Pediatr Neurosurg 43:236–248. https://doi.org/10.1159/000098836
7. Herman JM, McLone DG, Storrs BB, Dauser RC (1993) Analysis of 153 patients with myelomeningocele or spinal lipoma reoperated upon for a tethered cord. Presentation, management and outcome. Pediatr Neurosurg 19:243–249
8. Tani S, Yamada S, Knighton RS (1987) Extensibility of the lumbar and sacral cord. Pathophysiology of the tethered spinal cord in cats. J Neurosurg 66:116–123. https://doi.org/10.3171/jns.1987.66.1.0116
9. Kang JK, Kim MC, Kim DS, Song JU (1987) Effects of tethering on regional spinal cord blood flow and sensory-evoked potentials in growing cats. Childs Nerv Syst 3:35–39
10. Yamada S, Zinke DE, Sanders D (1981) Pathophysiology of "tethered cord syndrome". J Neurosurg 54:494–503. https://doi.org/10.3171/jns.1981.54.4.0494
11. Guthkelch AN, Pang DVJ (1981) Influence of closure technique on results in myelomeningocele. Childs Brain 8:350–355
12. Samuels R, McGirt MJ, Attenello FJ et al (2009) Incidence of symptomatic retethering after surgical management of pediatric tethered cord syndrome with or without duraplasty. Childs Nerv Syst 25:1085–1089. https://doi.org/10.1007/s00381-009-0895-6
13. Yamada S, Won DJ, Pezeshkpour G, Yamada BS, Yamada SM, Siddiqi J, Zouros A, Colohan ART (2007) Pathophysiology of tethered cord syndrome and similar complex disorders. Neurosurg Focus 23:1–10. https://doi.org/10.3171/FOC-07/08/E6
14. Dolan EJ, Transfeldt EE, Tator CH, Simmons EH, Hughes KF (1980) The effect of spinal distraction on regional spinal cord blood flow in cats. J Neurosurg 53:756–764. https://doi.org/10.3171/jns.1980.53.6.0756
15. Kocak A, Kilic A, Nurlu G et al (1997) A new model for tethered cord syndrome: a biochemical, electrophysiological, and electron microscopic study. Pediatr Neurosurg 26:120–126
16. Schneider SJ, Rosenthal AD, Greenberg BM, Danto J (1993) A preliminary report on the use of laser-Doppler flowmetry during tethered spinal cord release. Neurosurgery 32:214–218
17. Yamada S, Knerium DS, Mandybur GM, Schultz RL, Yamada BS (2004) Pathophysiology of tethered cord syndrome and other complex factors. Neurol Res 26:722–726. https://doi.org/10.1179/016164104225018027
18. Maurya VP, Rajappa M, Wadwekar V, Narayan SK, Barathi D, Madhugiri VS (2016) Tethered cord syndrome—a study of the short term effects of surgical detethering on markers of neuronal injury and electrophysiologic parameters. World Neurosurg. https://doi.org/10.1016/j.wneu.2016.07.005
19. Kowitzke B, Cohrs G, Leuschner I, Koch A, Synowitz M, Mehdorn HM, Held-Feindt J, Knerlich-Lukoschus F (2016) Cellular profiles and molecular mediators of lesion cascades in the placode in human open spinal neural tube defects. J Neuropathol Exp Neurol 75:827–842. https://doi.org/10.1093/jnen/nlw057
20. Kwon B, Kim DH, Vaccaro AR (2005) The pathophysiology of tethered cord syndrome: ischemia or apoptosis? Semin Spine Surg 17:8–12. https://doi.org/10.1053/j.semss.2005.01.001
21. Knerlich-Lukoschus F, Von Der Ropp-Brenner B, Lucius R et al (2010) Chemokine expression in the white matter spinal cord precursor niche after force-defined spinal cord contusion injuries in adult rats. Glia 58:916–931. https://doi.org/10.1002/glia.20974
22. Knerlich-Lukoschus F, Juraschek M, Blömer U, Lucius R, Mehdorn HM, Held-Feindt J (2008) Force-dependent development of neuropathic central pain and time-related CCL2/CCR2 expression after graded spinal cord contusion injuries of the rat. J Neurotrauma 25:427–448. https://doi.org/10.1089/neu.2007.0431
23. Qian BJ, You L, Shang FF, Liu J, Dai P, Lin N, He M, Liu R, Zhang Y, Xu Y, Zhang YH, Wang TH (2015) Vimentin regulates neuroplasticity in transected spinal cord rats associated with micRNA138. Mol Neurobiol 51:437–447. https://doi.org/10.1007/s12035-014-8745-2
24. Pineau I, Sun L, Bastien D, Lacroix S (2010) Astrocytes initiate inflammation in the injured mouse spinal cord by promoting the entry of neutrophils and inflammatory monocytes in an IL-1 receptor/MyD88-dependent fashion. Brain Behav Immun 24:540–553. https://doi.org/10.1016/j.bbi.2009.11.007
25. Reis JL, Correia-Pinto J, Monteiro MP, Costa M, Hutchins GM (2008) Vascular and apoptotic changes in the placode of myelomeningocele mice during the final stages of in utero

development. J Neurosurg Pediatr 2:150–157. https://doi.org/10.3171/PED/2008/2/8/150
26. Ribotta MGMG, Menet VV, Privat AA (2004) Glial scar and axonal regeneration in the CNS: lessons from GFAP and vimentin transgenic mice. Acta Neurochir Suppl 89:87–92. https://doi.org/10.1007/978-3-7091-0603-7_12
27. Pekny M, Wilhelmsson U, Pekna M (2014) The dual role of astrocyte activation and reactive gliosis. Neurosci Lett 565:30–38. https://doi.org/10.1016/j.neulet.2013.12.071
28. Herx LM, Rivest S, Yong VW (2000) Central nervous system-initiated inflammation and neurotrophism in trauma: IL-1 beta is required for the production of ciliary neurotrophic factor. J Immunol 165:2232–2239. https://doi.org/10.4049/jimmunol.165.4.2232
29. Bastien D, Lacroix S (2014) Cytokine pathways regulating glial and leukocyte function after spinal cord and peripheral nerve injury. Exp Neurol 258:62–77. https://doi.org/10.1016/j.expneurol.2014.04.006
30. Basu A, Krady JK, Levison SW (2004) Interleukin-1: a master regulator of neuroinflammation. J Neurosci Res 78:151–156. https://doi.org/10.1002/jnr.20266
31. Giulian D, Woodward J, Young DG, Krebs JF, Lachman LB (1988) Interleukin-1 injected into mammalian brain stimulates astrogliosis and neovascularization. J Neurosci 8:2485–2490
32. Sato A, Ohtaki H, Tsumuraya T, Song D, Ohara K, Asano M, Iwakura Y, Atsumi T, Shioda S (2012) Interleukin-1 participates in the classical and alternative activation of microglia/macrophages after spinal cord injury. J Neuroinflammation 9:65. https://doi.org/10.1186/1742-2094-9-65
33. Huang SL, Peng J, Yuan GL, Ding XY, He XJ, Lan BS (2015) A new model of tethered cord syndrome produced by slow traction. Sci Rep 5:9116. https://doi.org/10.1038/srep09116
34. Imtiyaz HZ, Simon MC (2010) Hypoxia-inducible factors as essential regulators of inflammation. Curr Top Microbiol Immunol 345:105–120. https://doi.org/10.1007/82-2010-74
35. Basu A, Lazovic J, Krady JK, Mauger DT, Rothstein RP, Smith MB, Levison SW (2005) Interleukin-1 and the interleukin-1 type 1 receptor are essential for the progressive neurodegeneration that ensues subsequent to a mild hypoxic/ischemic injury. J Cereb Blood Flow Metab 25:17–29. https://doi.org/10.1038/sj.jcbfm.9600002
36. Minami M, Kuraishi Y, Yabuuchi K, Yamazaki A, Satoh M (1992) Induction of interleukin-1 beta mRNA in rat brain after transient forebrain ischemia. J Neurochem 58:390–392
37. Legos JJ, Whitmore RG, Erhardt JA, Parsons AA, Tuma RF, Barone FC (2000) Quantitative changes in interleukin proteins following focal stroke in the rat. Neurosci Lett 282:189–192. https://doi.org/10.1016/S0304-3940(00)00907-1
38. Auron PE (1998) The interleukin 1 receptor: ligand interactions and signal transduction. Cytokine Growth Factor Rev 9:221–237. https://doi.org/10.1016/s1359-6101(98)00018-5
39. Dehne N, Brüne B (2009) HIF-1 in the inflammatory microenvironment. Exp Cell Res 315:1791–1797. https://doi.org/10.1016/j.yexcr.2009.03.019
40. Chen K-B, Uchida K, Nakajima H, Yayama T, Hirai T, Watanabe S, Guerrero AR, Kobayashi S, Ma WY, Liu SY, Baba H (2011) Tumor necrosis factor-α antagonist reduces apoptosis of neurons and oligodendroglia in rat spinal cord injury. Spine (Phila Pa 1976) 36:1350–1358. https://doi.org/10.1097/BRS.0b013e3181f014ec
41. Wajant H, Pfizenmaier K, Scheurich P (2003) Tumor necrosis factor signaling. Cell Death Differ 10:45–65. https://doi.org/10.1038/sj.cdd.4401189
42. Knerlich-Lukoschus F, Noack M, von der Ropp-Brenner B et al (2011) Spinal cord injuries induce changes in CB1 cannabinoid receptor and C-C chemokine expression in brain areas underlying circuitry of chronic pain conditions. J Neurotrauma 28:619–634. https://doi.org/10.1089/neu.2010.1652
43. Knerlich-Lukoschus F (2015) Chemokines and their receptors: important mediators to be aware of in neuroregenerative approaches for spinal cord injury. Neural Regen Res 10:562–564. https://doi.org/10.4103/1673-5374.155423
44. Cohrs G, Sürie J-P, Vokuhl C, Held-Feindt J, Synowitz M, Knerlich-Lukoschus F (2018) Establishing a retinoic induced mmc model in rats for investigating molecular lesion cascades during the post-neurulation fetal and perinatal development. Childs Nerv Syst 34:995–1094
45. Sharma U, Pal K, Pratap A, Gupta DK, Jagannathan NR (2006) Potential of proton magnetic resonance spectroscopy in the evaluation of patients with tethered cord syndrome following surgery. J Neurosurg 105:396–402. https://doi.org/10.3171/ped.2006.105.5.396
46. Pal K, Sharma U, Gupta DK, Pratap A, Jagannathan NR (2005) Metabolite profile of cerebrospinal fluid in patients with spina bifida: a proton magnetic resonance spectroscopy study. Spine (Phila Pa 1976) 30:E68–E72. https://doi.org/10.1097/01.brs.0000152161.08313.04
47. Baigrie RJ, Lamont PM, Kwiatkowski D, Dallman MJ, Morris PJ (1992) Systemic cytokine response after major surgery. Br J Surg 79:757–760. https://doi.org/10.1002/bjs.1800790813
48. Clementsen T, Krohn CD, Reikerås O (2006) Systemic and local cytokine patterns during total hip surgery. Scand J Clin Lab Invest 66:535–542. https://doi.org/10.1080/00365510600889635
49. Arishima Y, Setoguchi T, Yamaura I, Yone K, Komiya S (2006) Preventive effect of erythropoietin on spinal cord cell apoptosis following acute traumatic injury in rats. Spine (Phila Pa 1976) 31:2432–2438. https://doi.org/10.1097/01.brs.0000239124.41410.7a
50. Hattermann K, Knerlich-Lukoschus F, Lucius R, Mehdorn M, Held-Feindt J (2015) Erythropoietin and CCL3 antagonise their functional properties during neuroinflammation. Neurol Res 37:1025–1028. https://doi.org/10.1179/1743132815Y.0000000070
51. Yang L, Yan X, Xu Z, Tan W, Chen Z, Wu B (2016) Delayed administration of recombinant human erythropoietin reduces apoptosis and inflammation and promotes myelin repair and functional recovery following spinal cord compressive injury in rats. Restor Neurol Neurosci 34:647–663. https://doi.org/10.3233/RNN-150498